Received: 8 October 2020 | Revised: 9 April 2021 | Accepted: 1 June 2021

DOI: 10.1002/cjce.24252

ARTICLE

THE CANADIAN JOURNAL OF CHEMICAL ENGINEERING

Effect of Sn content on Pt/CNT electrocatalysts for direct ethanol fuel cell application

M. Florencia Azcoaga Chort | **Pablo A. Nagel** | **Natalia S. Veizaga** | **Virginia I. Rodríguez** | **Sergio R. de Miguel**

Instituto de Investigaciones en Catálisis y Petroquímica "Ing. José Miguel Parera" (INCAPE), Facultad de Ingeniería Química (UNL)-CONICET, Santa Fe, Argentina

Correspondence
Virginia I. Rodríguez, Instituto de Investigaciones en Catálisis y Petroquímica "Ing. José Miguel Parera" (INCAPE), Facultad de Ingeniería Química (UNL)-CONICET, 3000 Santa Fe, Argentina.
Email: virodri@fiq.unl.edu.ar

Abstract

Several bimetallic PtSn catalysts supported on multiwalled carbon nanotubes for ethanol electro-oxidation were prepared by conventional impregnation-reduction method. The Pt loading was kept at 20 wt.% and Pt:Sn atomic ratios of 5:1, 3:1, and 1:1 were selected. The catalysts were structurally characterized by temperature programmed reduction, X-ray diffraction, X-ray photoelectron spectroscopy, H_2 chemisorption, cyclohexane dehydrogenation reaction, and transmission electron microscopy. The electrochemical characterization of the electrocatalytic materials was carried out in acid medium by cyclic voltammetry, linear sweep voltammetry, chronoamperometry, and CO stripping techniques. Among the different stoichiometries tested, the Pt(20)Sn(12.17)/CNT catalyst exhibited the highest electrocatalytic activity for ethanol oxidation reaction, with mass current density of 189.5 mA $mgPt^{-1}$ at 796 mV (vs. Ag/AgCl).

KEYWORDS

carbon nanotubes, conventional impregnation, direct ethanol fuel cells, PtSn/CNT electrocatalysts

1 | INTRODUCTION

Fuel cells that use liquid alcohols, for instance, methanol and ethanol (direct-methanol fuel cells [DMFCs] and direct-ethanol fuel cells [DEFCs], respectively) are desirable as power sources for mobile and portable devices.[1–3] These alcohols are easy to handle, transport, and store, and no previous reformer system is needed to meet these ends.

Methanol is more easily oxidized than higher alcohols, but slow anode kinetics have been reported[4,5] and it has been regarded as a toxic product for a long time (mainly as a neurotoxin). On the one hand, ethanol is produced in large quantities from biomass and presents very low chemical toxicity. On the other hand, its complete oxidation into carbon dioxide is very complicated to achieve due to the C—C bond breaking and to the formation of CO intermediates that are responsible for poisoning Pt anode catalysts.[6–8]

Pt nanoparticles over different supports are usually employed as anode catalyst in DMFCs and DEFCs.[9–12] Pt surfaces initially show very high activity for alcohol oxidation, but they decline very rapidly in current, forming strongly bound intermediates.

The global mechanism of ethanol oxidation in acid solution may be represented as follows:

$$CH_3CH_2OH \rightarrow [CH_3CH_2OH]_{ads} \rightarrow C_{1ads} + C_{2ads} \rightarrow CO_2 \text{ (total oxidation)} \quad (R1)$$

$$CH_3CH_2OH \rightarrow [CH_3CH_2OH]_{ads} \rightarrow CH_3CHO \rightarrow CH_3COOH \text{ (partial oxidation)} \quad (R2)$$

where C_{1ads} and C_{2ads} represent the adsorbed intermediates on the electrode surface with one and two carbon atoms, respectively.[13]

 © 2021 Canadian Society for Chemical Engineering.

Nevertheless, pure Pt is rapidly poisoned on its surface by strongly adsorbed species coming from the ethanol dissociative adsorption, as mentioned before. Therefore, the addition of promoters to platinum mitigates Pt poisoning.[14–16] In this manner, several types of bimetallic Pt–M catalysts such as M = Ru,[17–20] Zn,[21] Fe,[22] Co,[23] Ni,[24–26] Sn,[26–40] Pr,[41], Rh,[37] and Pd[42] have been investigated as a replacement for pure Pt anodic catalyst in DEFC.

PtSn/C electrocatalyst performance depends greatly on the synthesis method, the Pt/Sn atomic ratio, and the coexistence of the alloy state of Pt and multivalent Sn.[13,39,43–45] In a research work conducted on bimetallic catalysts for ethanol oxidation reaction, Beyhan et al.[46] found that the PtSn/C catalyst was the best bimetallic catalyst in acidic media. This result is in line with the experiments done by Zhou et al.,[47] with PtSn/C exhibiting the highest peak in a cyclic voltammetry (CV) test compared to the bimetallic couples PtPd, PtW, and PtRu, and the monometallic catalyst. As was stated by Rousseau et al.,[48] the addition of Sn to Pt increases the catalyst activity towards ethanol oxidation and changes the product distribution, enhancing the ethanol oxidation to acetaldehyde and acetic acid.[48]

Controversial results on the effects of the Sn content and its state (alloyed or SnOx) in the catalysts on fuel cell performance were published. Lamy et al.[43] prepared PtSn/Vulcan XC-72 catalysts employing the Bönneman method with Pt:Sn atomic ratios of 3:1, 4:1, and 9:1. They observed an optimum Sn composition in the range of 10–20 wt.%. Several PtSn/Vulcan XC-72 catalysts with distinct nominal Pt:Sn ratios (1:1; 1:3, 2:1, 3:1, 4:1, and 9:1) were prepared by chemical reduction with formic acid as the reducing agent by Colmati et al.[36] The best performance of a DEFC among all materials studied was obtained using Pt_3Sn_1/C thermally treated at 200°C. Zignani et al.[49] prepared several PtSn/C catalysts by reduction of Pt and Sn precursors with formic acid. The catalyst with bulk composition Pt_3Sn_1 and a low concentration of reducing agent showed the best electrochemical performance. Conversely, Zhou et al.[47] prepared PtSn/Vulcan XC-72 electrocatalysts by polyol method with different Pt/Sn atomic ratios. The tests on a DEFC showed that Pt_2Sn_1/C, Pt_3Sn_2/C, or Pt_1Sn_1/C was better than Pt_3Sn_1/C or Pt_4Sn_1/C as a result of $-OH_{ads}$ supplying.

Within the above scope, the present work aims at determining the best Pt/Sn atomic ratio for PtSn/CNT catalysts prepared by conventional impregnation method to be used as anode electrocatalysts in low-temperature fuel cells. A comparison of the PtSn catalysts with different Pt/Sn atomic ratios was performed by the implementation of different techniques: X-ray diffraction (XRD), X-ray photoelectron spectroscopy (XPS), temperature programmed reduction (TPR), hydrogen chemisorption, cyclohexane dehydrogenation reaction (CHD), transmission electron microscopy (TEM), CO stripping, linear sweep voltammetry (LSV), cyclic voltammetry (CV), and chronoamperometry in ethanol solution electrolyte. The originality of this study is that it sheds light on the influence of Sn atomic ratio on the catalytic activity towards ethanol oxidation.

2 | EXPERIMENTAL

2.1 | Preparation of PtSn/CNT catalysts

PtSn bimetallic electrocatalysts (with Pt/Sn atomic ratios equal to 1:1, 3:1, and 5:1, i.e., 12.17, 4.06, and 2.43 wt.% Sn. respectively) were synthesized through a conventional impregnation method employing $H_2PtCl_6 \cdot 6H_2O$ (Tetrahedron) and $SnCl_2 \cdot 2H_2O$ (Cicarelli) as metallic precursors. The Pt nominal loading was 20 wt.%.

Multiwalled carbon nanotubes (CNTs) from Sunnano (purity > 90%, diameter: 10–30 nm, length: 1–10 μm, $S_{BET} = 211\ m^2g^{-1}$, and $V_{pore} = 0.46\ cm^3g^{-1}$) were employed as support. Before the synthesis, these nanotubes were purified to remove all inorganic impurities by subsequent treatments with aqueous solutions (10 wt.%) of HCl, HNO_3, and HF at 30°C for 48 h following the procedure presented by Vilella et al.[50] After HCl and HNO_3 treatments, CNTs were washed with deionized water up to a final pH value of 4. After HF treatment, CNTs were washed with deionized water up to the final pH of this water and then dried at 120°C for 24 h. A thermal treatment under hydrogen flow at 850°C for 4 h was performed to remove sulphur compounds.[50]

During the conventional impregnation/reduction method (CI),[51,52] CNTs were added to a stirred solution of Pt and Sn precursors, employing a solution volume/support mass ratio equal to 30 ml g^{-1}. The suspension was stirred at room temperature for 6 h and then heated to evaporation to ensure a complete metal deposition on CNTs. Finally, the catalyst reduction was performed at 230°C for 2 h under hydrogen flow.[53] For comparison purposes, Pt/CNT catalyst was also synthesized.

2.2 | Catalyst characterizations

2.2.1 | Structural analysis

Temperature programmed reduction (TPR)

After metal deposition, catalyst precursors were submitted to TPR experiments. Approximately 100 mg of sample were loaded in the reactor and heated to 800°C in a flow of H_2/N_2 at a ramp of 6°C min^{-1}. The hydrogen

consumption was monitored using a thermal conductivity detector (TCD).

X-ray diffraction (XRD)

The catalysts were characterized by XRD on a Shimadzu model XD3A spectrometer using Cu K α ($\lambda = 1.542 \times 10^{-10}$ m) radiation. The scanning range was from 20–100° and the scan rate was 2° min^{-1}.

X-ray photoelectron spectroscopy (XPS)

XPS of various catalysts were recorded on a Multitechnic Specs Photoemission Electron Spectrometer. The spectrometer operates with an energy power of 100 eV and the spectra were obtained with pass energy of 30 eV and a Mg anode operated at 90 W. The analysis chamber was kept at pressure lower than 2×10^{-6} Pa. The binding energies (BEs) of the signals were referred to the C1s peak at 284 eV. Peak area values were estimated by fitting the signals with a combination of Lorentzian–Gaussian curves of variable proportion and using the CasaXPS Peak Fit software version 1.

Hydrogen chemisorption

A volumetric equipment was employed to measure H_2 chemisorption at room temperature. The samples were previously outgassed at 1.3×10^{-2} Pa and 100°C for 30 min. The hydrogen adsorption isotherms were performed between 3.33×10^3–1.33×10^4 Pa, being linear in this range of pressure. Hydrogen chemisorption capacities were calculated by extrapolation of the isotherms to zero pressure.

Cyclohexane dehydrogenation reaction (CHD)

The reaction was carried out in a differential continuous flow reactor, being the catalysts previously reduced in situ in a flowing hydrogen atmosphere at 270°C for 2 h. The molar ratio H_2/CH was 26 and the total flow rate was 6 ml min^{-1}. The reaction products and the remaining reactants were analyzed by using a gas chromatographic system. The activation energy values for CHD (Ea_{CHD}) were estimated by linear regression with the help of the Arrhenius plot at three different reaction temperatures (240, 255, and 270°C).

Transmission electron microscopy (TEM)

TEM measurements were conducted on a JEOL 100CX microscope, operating at 100 kV, and magnification ranges of 80 000× and 100 000×. More than 200 particles were counted to obtain the distribution of particle sizes and the mean particle diameter.

2.2.2 | Electrochemical measurements

Electrochemical studies of the catalysts were carried out in a potentiostat/galvanostat (TEQ-02, Argentina) and a three-electrode test cell at room temperature. The reference electrode was an Ag/AgCl electrode, and the counter electrode was a Pt wire. An amount of 20 mg of the electrocatalyst was added to a mixture of 500 μl of acetone and 80 μl of Nafion. The mixture was sonicated for 15 min and 8 μl of this ink was added on the vitreous carbon disk electrode (4 mm diameter). Nitrogen was purged through the electrolyte solution for 10 min to remove oxygen before conducting each experiment, while a nitrogen atmosphere was maintained during the measurements.

Cyclic voltammetry (CV)

Electrochemical activities towards ethanol oxidation were measured in 0.5 mol/L H_2SO_4 + 1 mol/L C_2H_5OH solution. The CVs were recorded in the range of −200 and 1200 mV (vs. Ag/AgCl) at a scan rate of 25 mV s^{-1}.

Linear sweep voltammetry (LSV)

The LSV test was performed in deaerated 0.5 mol/L H_2SO_4 + 1 mol/L C_2H_5OH solution at a scan rate of 1 mV s^{-1}.

Chronoamperometric measurements

The temporal stability at 350 mV (vs. Ag/AgCl) was determined by chronoamperometry in a solution of 0.5 mol/L H_2SO_4 + 1 mol/L C_2H_5OH for 60 min.

CO stripping

CO was bubbled in the electrolytic solution (0.5 mol/L H_2SO_4) for 60 min at a constant potential of 200 mV (vs. Ag/AgCl). Then, N_2 was passed to purge the electrolytic solution to eliminate the dissolved CO. Afterwards, N_2 was bubbled to remove CO traces from the gas phase. The electrochemical active surface area (ECSA) was obtained from the CO voltammetry.

3 | RESULTS AND DISCUSSION

Figure 1 shows TPR profiles of Pt/CNT and PtSn/CNT catalyst precursors prepared by the conventional impregnation method. A TPR profile of Sn (12.17 wt.%)/CNT is also included. For the sake of comparison, a blank experiment was also performed using pure CNT.

The TPR profile of the support (CNT) does not exhibit signals corresponding to hydrogen consumption, which indicates that practically no functional groups are present on the carbonaceous surface. The Pt/CNT catalyst (see Figure 1) exhibits a narrow peak at about 200°C corresponding to the reduction of the oxychloro platinum species originated after the impregnation of the CNTs with H_2PtCl_6 and the following drying step.[54]

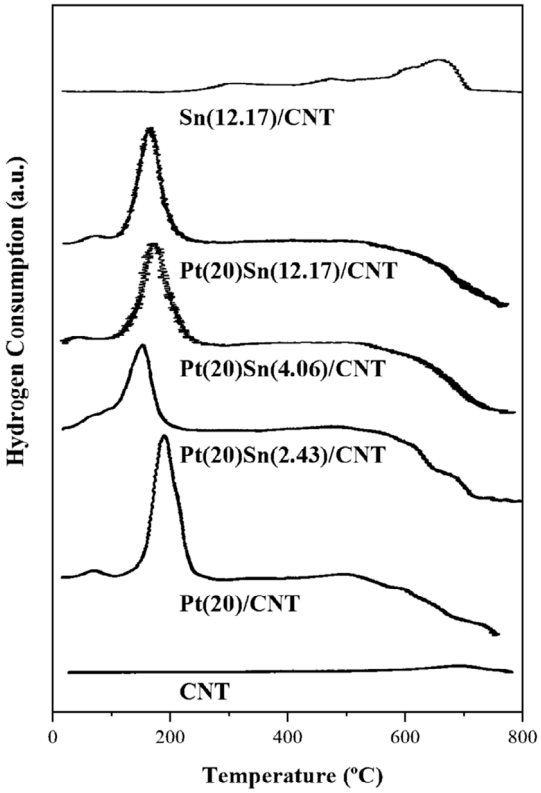

FIGURE 1 Temperature programmed reduction (TPR) profiles of Pt/CNT, Sn/CNT, and PtSn/CNT catalysts

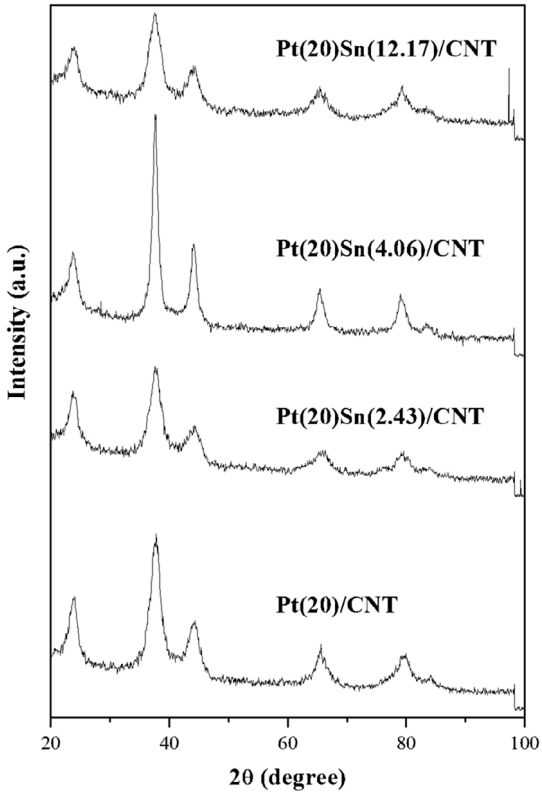

FIGURE 2 X-ray diffraction (XRD) profiles of Pt/CNT and PtSn/CNT catalysts

On the contrary, the Sn/CNT catalyst displays a small reduction zone at very high temperatures (>600°C). This is due to the reduction of small amounts of Sn species, in a similar way to that observed in the TPR profile of $Sn/MgAl_2O_4$ catalyst.[55] By comparing the profiles corresponding to PtSn/CNT samples of different Sn concentrations with that of the Pt/CNT, it can be observed in Figure 1 that the peaks of the bimetallic samples are wider and that the maximum of the peak is shifted to lower values with Sn addition. In this sense, this TPR signal appears at temperatures between 160–180°C. Besides, no reduction zone at high temperatures (like in Sn/CNT) appears in any of the bimetallic catalysts, indicating that a fraction of Sn species would be correduced with Pt at very low temperatures. Such correduction could lead to probable PtSn alloy formation.

Figure 2 displays X-ray diffractograms of mono- and bimetallic electrocatalysts supported on CNT. The broad peak at about 20–25° is associated with CNT support material. The observed peaks at $2\theta = 39.8$, 46.3, 67.5, and 81.6° indicate face-centred cubic structures (fcc) typical of metallic platinum represented by (111), (200), (220), and (311) planes, respectively.

The sizes of the crystallites were determined by the widening of the diffraction peaks. Table 1 shows the results of the medium crystallite sizes obtained by the Scherrer formula from the widening of the (220) peak of 67.5° and the lattice parameter (a). The values of the crystallite sizes are similar for all the catalysts, except for the bimetallic catalyst with 4.06 wt.% Sn, which is larger than the other samples. It should be noted that XRD is not a completely accurate technique for determining crystallite sizes smaller than 5 nm. In comparison to the lattice parameter of bulk Pt (0.392 3 nm, JCPDS 040802) and nanometre Pt (0.391 5 nm),[47] the corresponding values of the three bimetallic catalysts slightly increased with tin addition to the catalyst. This result seems to indicate that part of Sn entered the crystal lattice of Pt, and it was consequently modified. This is compatible with alloy formation between Sn and Pt,[56] in agreement with TPR results.

Oxidation states of Sn in the surface layers of PtSn/CNT catalysts were studied through XPS. This was done since their XRD patterns are not sharp enough to determine the present phases. Figure 3 shows XPS spectra of Sn 3d regions in Pt(20)Sn(4.06)/CNT catalyst.

From the deconvolution of the Sn 3d region of XPS spectra, two pairs of peaks were obtained: two very small peaks located at 485.6 and 494 eV assigned to zerovalent Sn, and two important peaks at 487 and 496 eV, which

TABLE 1 Values of crystallite size and lattice parameter determined by X-ray diffraction (XRD), hydrogen chemisorption (H), initial reaction rate (R_{CH}^0), and activation energy (Ea_{CH}) for cyclohexane dehydrogenation reaction for Pt/CNT and PtSn/CNT catalysts

Catalyst	Crystallite size (nm)	Lattice parameter (nm)	H (μmol H_2 gcat^{-1})	R_{CH}^0 (mol h^{-1} gPt^{-1})	Ea_{CH} (kcal mol^{-1})
Pt(20)/CNT	4.0	0.391 5	121	6.7	40.0
Pt(20)Sn(2.43)/CNT	3.0	0.391 9	154	5.8	38.8
Pt(20)Sn(4.06)/CNT	5.7	0.392 5	128	6.9	38.3
Pt(20)Sn(12.17)/CNT	3.3	0.393 0	134	5.7	37.2

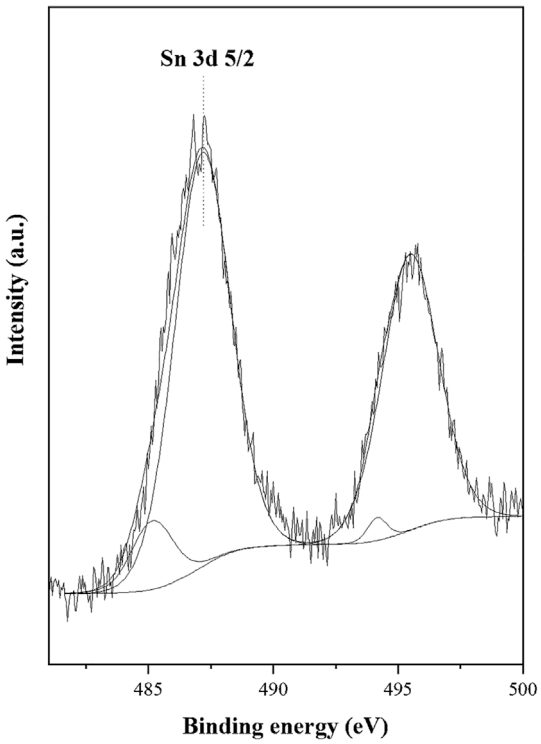

FIGURE 3 Sn 3d X-ray photoelectron spectroscopy (XPS) signals of Pt(20)Sn(4.06)/CNT catalyst

are the characteristic peaks of Sn(II)/(IV) oxidized species. It must be noted that Sn(II) and Sn(IV) species cannot be discriminated because their binding energies are very similar.[57] In this case, the reduction of Sn(IV) species to the zerovalent state under flowing hydrogen is expected to be harder to achieve. A very low amount of Sn(0) (7%) was found after the reduction step, with this small metallic fraction possibly forming alloys with metallic Pt. Similar results were found by Veizaga et al.[58] This result indicates that Sn mainly exists in the form of SnO, SnO_2, or Sn hydroxides. Concerning the reduction degree of Pt in this bimetallic sample, Pt 4f spectrum (not shown here) indicated that most of the Pt was in a zerovalent state (>65%) and a small portion was forming oxidized species of Pt. In agreement with our work, Kim et al.[59] reported XPS spectra of Pt 4f and Sn 3d for Pt and PtSn catalysts. They found that Pt(0) is the predominant species in all bimetallic catalysts, with small quantities of oxidized Pt species. A binding energy shift to lower energies by 0.3–1.0 eV appeared in all bimetallic catalysts compared to the monometallic one, due to electronegativity differences in the elemental Pt and Sn, leading to charge transfer from the less-electronegative Sn to the more-electronegative Pt. For XPS spectra of Sn 3d, it was found that the Sn surface state is oxidic (e.g., SnO, SnO_2, or Sn hydroxides), regardless of the Sn content in the bimetallic catalysts.

Hydrogen chemisorption capacities of mono- and bimetallic electrocatalyst are presented in Table 1. PtSn/CNT catalysts prepared by conventional impregnation method showed similar hydrogen chemisorption values to that of the corresponding Pt/CNT. Table 1 also presents the values of initial reaction rates and activation energies in CHD for the synthesized catalysts. Considering that this metallic phase test reaction is a structure-insensitive reaction, changes in activation energy in CHD (Ea_{CH}) can be related to electronic modifications of the active sites.[60] The activation energy values of the bimetallic catalysts are slightly lower than that of Pt/CNT (see Table 1). This would indicate that the electronic effects of Sn on Pt sites take place in these PtSn/CNT catalysts. Taking into account the characteristics of CHD, this is a reaction that is carried out on one surface active atom of the catalyst; for this reason, CHD is an indirect measurement of exposed surface Pt atoms. Table 1 also shows that the initial CHD reaction rate values are similar to those of the corresponding monometallic ones. These results are in agreement with the similar chemisorption values shown in the same table.

TEM was employed to examine the morphological structure, particle size, and dispersion of mono- and bimetallic catalysts. Figure 4 shows a TEM image and the particle size distribution for each of the four catalysts.

Besides, Figure 4 presents the mean particle size values for all the catalysts. TEM results indicate that all PtSn/CNT catalysts display similar mean particle sizes to Pt/CNT, according to chemisorption and test reaction results. In this respect, the CI method would assure a strong interaction between the CNTs and the metallic precursor during impregnation, leading to higher

dispersions of the metallic phase. Concerning the distributions of particle sizes, they are also similar for mono- and bimetallic catalysts, showing the majority of the sizes between 2–3.5 nm.

Taking into account the characterization results, TPR results indicate that a fraction of Sn species would be co-reduced with Pt at very low temperatures, which could be due not only to the presence of geometric effects but also to electronic ones of Sn on Pt, such as was determined by a structure-insensitive test reaction like CHD. It could be determined that the active metal exhibits strong interactions not only with the promoter but also with the support, giving rise to high metallic dispersions and small particle sizes, such as those observed by TEM.

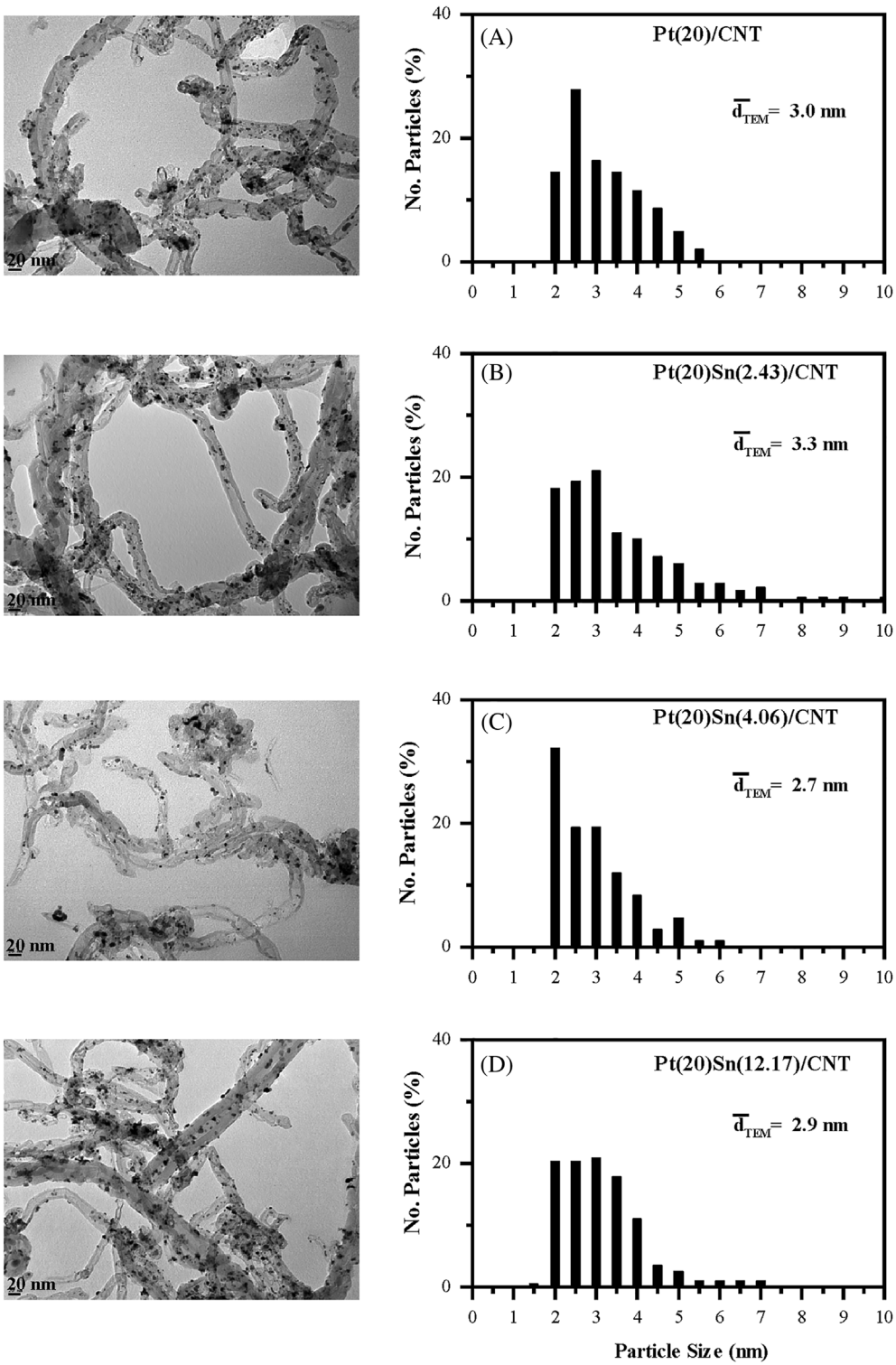

FIGURE 4 Transmission electron microscopy (TEM) images and particle size distributions of (A) Pt(20)/CNT, (B) Pt(20)Sn(2.43)/CNT, (C) Pt(20)Sn(4.06)/CNT, and (D) Pt(20)Sn(12.17)/CNT catalysts

TABLE 2 Values of onset potential of CO oxidation ($E_{CO,\ Onset}$) and electrochemical active surface area (ECSA) of Pt/CNT and PtSn/CNT catalysts

Catalyst	$E_{CO,Onset}$ (mV [vs. Ag/AgCl])	ECSA ($m^2\ gPt^{-1}$)
Pt(20)/CNT	411	43.6
Pt(20)Sn(2.43)/CNT	225	32.0
Pt(20)Sn(4.06)/CNT	215	43.5
Pt(20)Sn(12.17)/CNT	190	51.6

Despite the very high metallic charges deposited on the CNTs by conventional impregnation, the mean particle diameters for all the catalysts ranged between 2.7–3.3 nm.

Table 2 presents both the CO oxidation onset potentials and the ECSA of PtSn catalysts compared with Pt/CNT. It is evident that the beginning of the CO oxidation is displaced to lower potentials for all PtSn catalysts (from 411–190 mV vs. Ag/AgCl). The earlier oxidation of CO_{ads} in Sn containing electrodes, compared with the corresponding Pt one, could be explained by the Sn ability to adsorb OH at more negative potentials than Pt; it could also be explained by the reactions of surrounding CO_{ads} species over Pt sites (bifunctional mechanism) or the modification of the d electronic Pt bands by Sn.[47] As stated by the electro-oxidation bifunctional mechanism,[34,61] the synergistic effect is a result of the fact that Sn activates water molecules and provides preferential sites for $-OH_{ads}$ adsorption at lower potentials than Pt. Abundant $-OH_{ads}$ species are necessary to completely oxidize the poisoning intermediates to CO_2.

Characterization and CO stripping results indicate that there are promoting effects of Sn over Pt in these catalysts. This fact could be explained by the presence of geometric modifications caused by Sn placed in the vicinity of the active metallic phase. As displayed by XRD results, the addition of Sn could induce the extension of Pt–Pt distance. The extended Pt–Pt distance could ease the dissociative adsorption of much bigger ethanol molecules at a lower potential region and thus enhance the ethanol oxidation.[62] These promoting effects of Sn on Pt would ease the oxidation of CO to CO_2 at lower potentials. Following the same trend that reflected TEM, H_2 chemisorption, and CHD results, Table 2 shows that ECSA values for bimetallic catalysts supported on CNT are comparable to those of the monometallic electrocatalyst.

For the evaluation of the ethanol oxidation activity, CV curves were recorded (Figure 5) at a scan rate of 25 mV s^{-1} with a potential scanning from −200–1200 mV (vs. Ag/AgCl) at room temperature. The curves stabilized after five cycles and no severe changes in the shape or size of the voltammograms were detected.

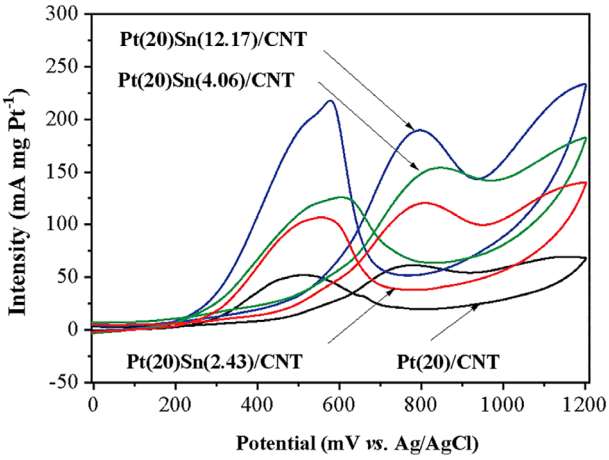

FIGURE 5 Cyclic voltammograms of Pt/CNT and PtSn/CNT catalysts, recorded in 0.5 mol/L H_2SO_4 with 1 mol/L C_2H_5OH at a scan rate of 25 mV s^{-1}

The Pt loading was kept at 20 wt.% and the current densities were normalized by Pt mass.

Two oxidation current peaks appear on the forward and backward scan (Figure 5). The oxidation peak in the forward scan corresponds to the oxidation of freshly chemisorbed species coming from ethanol adsorption, although the oxidation peak in the reverse scan corresponds mainly to the oxidative removal of adsorbed carbonaceous species.[63]

When analyzing the applied potential in CV experiments, it can be seen that ethanol oxidation is almost completely hindered by the poisoning of adsorbed carbonaceous intermediates when the applied potential is below 200 mV (vs. Ag/AgCl). Above this potential, these intermediates start to be oxidized at an appreciable rate, leading to a peak in the forward scan. At higher potentials, the reaction is first inhibited by Pt oxides formation and then increases again at ∼900–950 mV (vs. Ag/AgCl) due to the generation of Pt-OH, which helps the removal of CO poisoning species. In the backward scan, after the reduction of Pt oxide, the anodic peak at ∼500–550 mV (vs. Ag/AgCl) is due to the oxidation of remaining residues at the surface.

By comparing CV curves (Table 3), Sn addition to Pt leads to significant increases in the catalytic activity for the ethanol oxidation, in agreement with previously reported data.[64,65] The peak current densities are improved over all bimetallic catalysts compared to the corresponding Pt/CNT catalyst, hinting that Sn additions to Pt could improve the reaction rate despite Sn contents up to 12%.

The performance of Pt(20)Sn(12.17)/CNT catalyst is the best for all catalysts prepared for ethanol oxidation. The anodic peak current occurs at 796 mV (vs. Ag/AgCl), and the peak current density is 189.5 mA $mgPt^{-1}$ during positive potential scanning on this catalyst.

TABLE 3 Cyclic voltammetry (CV) results of Pt/CNT and PtSn/CNT catalysts for ethanol oxidation reaction

Catalyst	Positive peak potential (mV [vs. Ag/AgCl])	Positive peak current (mA $mgPt^{-1}$)	Onset potential (mV [vs. Ag/AgCl])
Pt(20)/CNT	780	61.0	181
Pt(20)Sn(2.43)/CNT	811	120.5	127
Pt(20)Sn(4.06)/CNT	842	153.5	112
Pt(20)Sn(12.17)/CNT	796	189.5	101

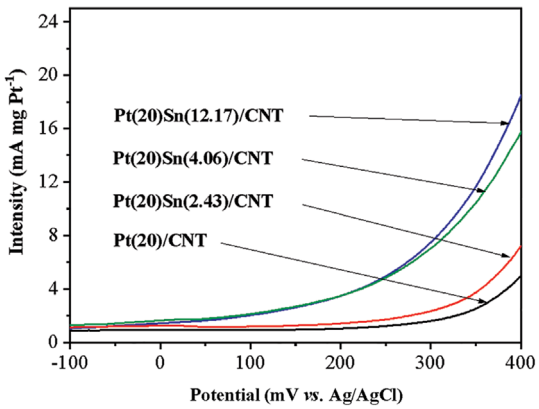

FIGURE 6 Linear sweep voltammetry (LSV) curves of Pt/CNT and PtSn/CNT catalysts, recorded in 0.5 mol/L H_2SO_4 with 1 mol/L C_2H_5OH at a scan rate of 1 mV s^{-1}

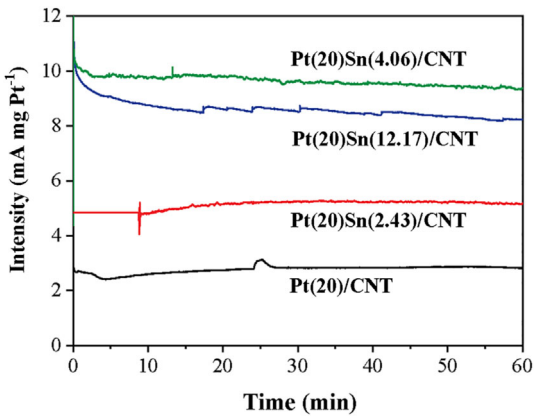

FIGURE 7 Chronoamperometry curves of Pt/CNT and PtSn/CNT catalysts, recorded in 0.5 mol/L H_2SO_4 with 1 mol/L C_2H_5OH

Table 3 also shows the onset potential values (fixed at the potential where the slope of the curves exceeded 15% determined from LSV curves shown in Figure 6) and the maximum current density.

The onset potential always decreases with the addition of the secondary metal. According to the electrochemical principle, the electrocatalytic activity is determined by the basic physical properties of the surface active sites. With the increase of the Sn content, the electronegativity difference in the metal element changes the electronic properties of Pt and weakens the adsorption of carbonaceous intermediates.[66] The lowest onset potential of ethanol oxidation value is found for Pt(20)Sn(12.17)/CNT catalyst, indicating that the energy required for ethanol oxidation on this catalyst is lower. This fact could be assigned to both the Pt and Sn interaction (electronic effect) and the slight changes in the Pt lattice parameter (structural effect) due to the addition of Sn.[67,68] The probable presence of alloyed Sn expanding the lattice would allow ethanol to be adsorbed and dissociated at lower potentials than the one observed on the corresponding monometallic catalyst. Besides, the presence of Sn oxide in the vicinity of Pt particles may contribute to the promotion of ethanol oxidation at lower potentials and increase the reaction rate. Additionally, Figure 5 shows that the onset potential shifts towards lower values when the Sn content is increased from 2% to 12%.

Chronoamperometric experiments were conducted by holding the potential at 350 mV (vs. Ag/AgCl) for 60 min in 0.5 mol/L H_2SO_4 containing 1 mol/L CH_3CH_2OH, and the results are presented in Figure 7. The current of all PtSn catalysts drops rapidly within 5 min and then decays slowly. After holding the potential for 60 min, the following order is observed: Pt(20)Sn(4.06)/CNT ≅ Pt(20)Sn(12.17)/CNT > Pt(20)Sn(2.43)/CNT > Pt(20)/CNT. For ethanol oxidation, Pt(20)Sn(4.06)/CNT and Pt(20)Sn(12.17)/CNT catalysts exhibit the maximum current intensities at 9.3 and 8.2 mA $mgPt^{-1}$, respectively.

4 | CONCLUSIONS

Pt and PtSn nanoparticles supported on multiwalled CNTs were prepared by conventional impregnation-reduction method. TEM characterization showed that the addition of Sn has a minor influence on particle size. According to XRD patterns, the lattice parameter of PtSn/CNT catalysts increased with the increment of Sn content, suggesting the formation of a PtSn alloy in the catalysts. This effect was also observed by TPR and cyclohexane dehydrogenation reaction measurements. CV measurements showed that the atomic ratio of 1:1 was

the optimum ratio for PtSn/CNT catalyst. The increase of performance of Pt(20)Sn(12.17)/CNT electrocatalyst could be attributed to the effect of tin oxides adjacent to Pt sites, which favours the oxidation of adsorbed intermediates by the bifunctional mechanism.

ACKNOWLEDGEMENTS

The authors thank Universidad Nacional del Litoral, CONICET, and ANPCyT.

ORCID

M. Florencia Azcoaga Chort https://orcid.org/0000-0001-9908-5726
Pablo A. Nagel https://orcid.org/0000-0001-7324-4063
Natalia S. Veizaga https://orcid.org/0000-0002-5692-0071
Virginia I. Rodríguez https://orcid.org/0000-0002-4597-9844
Sergio R. de Miguel https://orcid.org/0000-0002-6132-8136

REFERENCES

[1] M. A. F. Akhairi, S. K. Kamarudin, *Int. J. Hydrogen Energ.* **2016**, *41*, 4214.
[2] E. Antolini, E. Gonzalez, *Electrochim. Acta* **2010**, *56*, 1.
[3] L. Jiang, G. Sun, *Progress in Electrocatalysts for Direct Alcohol Fuel Cells*, 1st ed., Wiley-VCH, Weinheim, Germany **2015**, p. 215.
[4] H. Liu, C. Song, L. Zhang, J. Zhang, H. Wang, D. P. Wilkinson, *J. Power Sources* **2006**, *155*, 95.
[5] R. G. C. S. dos Reis, F. Colmati, *J. Solid State Electr.* **2016**, *20*, 2559.
[6] S. C. Chang, L. W. Leung, M. J. Weaver, *J. Phys. Chem.* **1990**, *94*, 6013.
[7] E. Antolini, *J. Power Sources* **2007**, *170*, 1.
[8] J. C. M. Silva, B. Anea, R. F. B. de Souza, M. H. M. T. Assumpção, M. L. Calegaro, A. O. Neto, M. C. Santos, *J. Brazil. Chem. Soc.* **2013**, *24*, 1553.
[9] S. Basri, S. K. Kamarudin, W. R. W. Daud, Z. Yaakub, *Int. J. Hydrogen Energ.* **2010**, *35*, 7957.
[10] A. M. Zainoodin, S. K. Kamarudin, W. R. W. Daud, *Int. J. Hydrogen Energ.* **2010**, *35*, 4606.
[11] M. Z. F. Kamarudin, S. K. Kamarudin, M. S. Masdar, W. R. K. Daud, *Int. J. Hydrogen Energ.* **2013**, *38*, 9438.
[12] S. S. Siwal, S. Thakur, Q. B. Zhang, V. K. Thakur, *Materials Today Chemistry* **2019**, *14*, 100182.
[13] E. Antolini, E. R. Gonzalez, *Catal. Today* **2011**, *160*, 28.
[14] S. Song, P. Tsiakaras, *Appl. Catal. B-Environ.* **2006**, *63*, 187.
[15] H. Su, T.-H. Chen, *Chinese Chem. Lett.* **2016**, *27*, 1083.
[16] M. C. Figueiredo, O. Sorsa, N. Doan, E. Pohjalainen, H. Hildebrand, P. Schmuki, B. P. Wilson, T. Kallio, *J. Power Sources* **2015**, *275*, 341.
[17] F. G. Carbajal, M. A. García, S. A. Gamboa, *J. New Mat. Electr. Sys.* **2018**, *21*, 43.
[18] Y. V. Tolmachev, O. A. Petrii, *J. Solid State Electr.* **2017**, *21*, 613.
[19] O. Sahin, D. Duzenli, H. Kivrak, *Energ. Source. Part A* **2016**, *38*, 628.
[20] Y. Zhao, Y. Maswadeh, S. Shan, H. Cronk, Z. Skeete, B. Prasai, J. Luo, V. Petkov, C.-J. Zhong, *J. Phys. Chem. C* **2017**, *121*, 17077.
[21] H.-X. Zhao, S.-M. Wang, D.-Q. Xue, Y.-J. Chen, *Journal of Fuel Chemistry and Technology* **2011**, *39*, 140.
[22] N. A. Tapan, Ö. Yildiz, *Int. J. Chem. React. Eng.* **2010**, *8*, A160.
[23] F. Wang, J. Qiao, H. Wu, J. Qi, W. Li, Z. Mao, Z. Wang, W. Sun, D. Rooney, K. Sun, *Chem. Eng. J.* **2017**, *317*, 623.
[24] J. E. Sulaiman, S. Zhu, Z. Xing, Q. Chang, M. Shao, *ACS Catal.* **2017**, *7*, 5134.
[25] E. Antolini, *Energies* **2017**, *10*, 1.
[26] K. Ponmani, S. Kiruthika, B. Muthukumaran, *J. Electrochem. Sci. Te.* **2015**, *6*, 95.
[27] N. Mahamai, T. Promanan, T. Sarakonsri, *Mater. Today-Proc.* **2019**, *17*, 1561.
[28] X. Wang, H. Xue, L. Yang, H. Wang, P. Zang, X. Qin, Y. Wang, Y. Ma, Q. Wu, Z. Hu, *Nanotechnology* **2011**, *22*, 395401.
[29] S. S. Gwebu, P. N. Nomngongo, N. W. Maxakato, *Electroanal.* **2018**, *30*, 1125.
[30] V. I. Rodríguez, N. S. Veizaga, S. R. De Miguel, *J. Electrochem. Soc.* **2017**, *164*, F1524.
[31] P. G. Corradini, N. A. Santos, J. Perez, *Fuel Cells* **2018**, *18*, 73.
[32] J. Liu, Z. Li, C. He, R. Fu, D. Wu, S. Song, *Int. J. Hydrogen Energ.* **2011**, *36*, 2250.
[33] Y. Wang, S. Song, G. Andreadis, H. Liu, P. Tsiakaras, *J. Power Sources* **2011**, *196*, 4980.
[34] S.-Y. Yan, Y.-R. Huang, C.-Y. Yang, C.-W. Liu, J.-H. Wang, K.-W. Wang, *Electrochim. Acta* **2018**, *259*, 733.
[35] T.-H. Huangwang, H.-S. Zheng, Y.-M. Cheng, C.-W. Liu, S.-W. Lee, J.-H. Wang, K.-W. Wang, *Sustainable Energy and Fuels* **2019**, *3*, 3352.
[36] F. Colmati, M. M. Magalhães, R. Sousa Jr., E. G. Ciapina, E. R. Gonzalez, *Int. J. Hydrogen Energ.* **2019**, *44*, 28812.
[37] S. Song, C. He, J. Liu, Y. Wang, A. Brouzgou, P. Tsiakaras, *Appl. Catal. B-Environ.* **2012**, *119*, 227.
[38] Y. Liu, M. Wei, D. Raciti, Y. Wang, P. Hu, J. H. Park, M. Barclay, C. Wang, *ACS Catal.* **2018**, *8*, 10931.
[39] J. Asgardia, J. C. Calderón, F. Alcaide, A. Querejeta, L. Calvillo, M. J. Lázaro, G. García, E. Pastora, *Appl. Catal. B-Environ.* **2015**, *168*, 33.
[40] N. Hidayati, K. Scott, *Bulletin of Chemical Reaction Engineering and Catalysis* **2016**, *11*, 10.
[41] P. G. Corradini, E. Antolini, J. Perez, *J. Power Sources* **2014**, *251*, 402.
[42] J. Seweryn, A. Lewera, *J. Power Sources* **2012**, *205*, 264.
[43] C. Lamy, S. Rousseau, E. M. Belgsir, C. Coutanceau, J.-M. Léger, *Electrochim. Acta* **2004**, *49*, 3901.
[44] L. Jiang, G. Sun, Z. Zhou, W. Zhou, Q. Xin, *Catal. Today* **2004**, *93–95*, 665.
[45] W. T. Napporn, H. Laborde, J.-M. Léger, C. Lamy, *J. Electroanal. Chem.* **1996**, *404*, 153.
[46] S. Beyhan, C. Countanceau, J.-M. Léger, W. T. Napporn, F. Kadirgan, *Int. J. Hydrogen Energ.* **2013**, *38*, 6830.
[47] W. Zhou, Z. Zhou, S. Song, W. Li, G. Sun, P. Tsiakaras, Q. Xin, *Appl. Catal. B-Environ.* **2003**, *46*, 273.
[48] S. Rousseau, C. Coutanceau, C. Lamy, J.-M. Léger, *J. Power Sources* **2006**, *158*, 18.
[49] S. C. Zignani, V. Baglio, J. J. Linares, G. Monforte, E. R. Gonzalez, A. S. Aricò, *Electrochim. Acta* **2012**, *70*, 255.

[50] I. M. J. Vilella, S. R. de Miguel, C. Salinas-Martínez de Lecea, Á. Linares-Solano, O. A. Scelza, *Appl. Catal. A-Gen.* **2005**, *281*, 247.
[51] M. C. Román-Martinez, D. Cazorla-Amorós, H. Yamashita, S. de Miguel, O. Scelza, *Langmuir* **2000**, *16*, 1123.
[52] N. Veizaga, J. Fernandez, M. Bruno, O. Scelza, S. de Miguel, *Int. J. Hydrogen Energ.* **2012**, *37*, 17910.
[53] S. R. de Miguel, J. I. Vilella, E. L. Jablonski, O. A. Scelza, C. . Salinas Martinez de Lecea, A. Linares-Solano, *Appl. Catal. A-Gen.* **2002**, *232*, 237.
[54] S. R. de Miguel, O. A. Scelza, M. C. Román-Martínez, C. Salinas-Martínez de Lecea, D. Cazorla-Amorós, A. Linares-Solano, *Appl. Catal. A-Gen.* **1998**, *170*, 93.
[55] S. A. Bocanegra, A. Guerrero-Ruiz, S. R. de Miguel, O. A. Scelza, *Appl. Catal. A-Gen.* **2004**, *277*, 11.
[56] E. Antolini, F. Colmati, E. R. Gonzalez, *Electrochem. Commun.* **2007**, *9*, 398.
[57] E. Janin, M. Björkqvit, T. M. Grehk, M. Göthelid, C.-M. Pradier, U. O. Karlsson, A. Rosengren, *Appl. Surf. Sci.* **1996**, *99*, 371.
[58] N. S. Veizaga, V. I. Rodriguez, T. A. Rocha, M. Bruno, O. A. Scelza, S. R. de Miguel, E. R. Gonzalez, *J. Electrochem. Soc.* **2015**, *162*, F243.
[59] J. H. Kim, S. M. Choi, S. H. Nam, M. H. Seo, S. H. Choi, W. B. Kim, *Appl. Catal. B-Environ.* **2008**, *82*, 89.
[60] G. L. Haller, *J. Catal.* **2003**, *216*, 12.
[61] B. R. Gurau, R. Viswanathan, R. X. Liu, T. J. Lafrenz, K. L. Ley, E. S. Smotkin, E. Reddington, A. Sapienza, B. C. Chan, T. E. Mallouk, S. Sarangapani, *J. Phys. Chem. B* **1998**, *102*, 9997.
[62] H. Li, G. Sun, L. Cao, L. Jiang, Q. Xin, *Electrochim. Acta* **2007**, *52*, 6622.
[63] K. Kakaei, *Electrochim. Acta* **2015**, *165*, 330.
[64] F. Vigier, C. Coutanceau, A. Perrard, E. M. Belgsir, C. Lamy, *J. Appl. Electrochem.* **2004**, *234*, 439.
[65] H. Wang, Z. Jusys, R. J. Behm, *J. Power Sources* **2006**, *154*, 351.
[66] Z. Wang, H. Fan, H. Liang, J. Ma, S. Li, Y. Song, R. Wang, *Electrochim. Acta* **2017**, *230*, 245.
[67] S. Mukerjee, J. McBreen, *J. Electrochem. Soc.* **1999**, *146*, 600.
[68] A. O. Neto, T. R. R. Vasconcelos, R. W. R. V. da Silva, M. Linardi, E. V. Spinace, *J. Appl. Electrochem.* **2005**, *35*, 193.

How to cite this article: M. F. Azcoaga Chort, P. A. Nagel, N. S. Veizaga, V. I. Rodríguez, S. R. de Miguel, *Can. J. Chem. Eng.* **2022**, *100*(8), 1848. https://doi.org/10.1002/cjce.24252